

# Environment-Aware Adaptive Pruning with Interleaved Inference Orchestration for Vision-Language-Action Models

Yuting Huang <sup>\*1</sup> Leilei Ding <sup>\*1</sup> Zhipeng Tang <sup>\*1</sup> Zenghuan Zhu <sup>1</sup> Jiajun Deng <sup>1</sup> Xinrui Lin <sup>1</sup> Shuo Liu <sup>1</sup>  
Haojie Ren <sup>1</sup> Jianmin Ji <sup>1</sup> Yanyong Zhang <sup>1</sup>

## Abstract

While Vision-Language-Action (VLA) models hold promise in embodied intelligence, their large parameter counts lead to substantial inference latency that hinders real-time manipulation, motivating parameter sparsification. However, as the environment evolves during VLA execution, the optimal sparsity patterns change accordingly. Static pruning lacks the adaptability required for environment dynamics, whereas fixed-interval dynamic layer pruning suffers from coarse granularity and high retraining overheads. To bridge this gap, we propose **EcoVLA**, a training-free, plug-and-play adaptive pruning framework that supports orthogonal combination with existing VLA acceleration methods. EcoVLA comprises two components: **Environment-aware Adaptive Pruning (EAP)** and **Interleaved Inference Orchestration (I<sup>2</sup>O)**. EAP is a lightweight adaptive channel pruning method that incorporates the temporal consistency of the physical environment to update sparsity patterns. I<sup>2</sup>O leverages the FLOPs bubbles inherent in VLA inference to schedule the pruning method in parallel, ensuring negligible impact on latency. Evaluated on diverse VLA models and benchmarks, EcoVLA delivers state-of-the-art performance, achieving up to 1.60 $\times$  speedup with only a 0.4% drop in success rate, and further reaches 2.18 $\times$  speedup with only a 0.5% degradation when combined with token pruning. We further validate the effectiveness of EcoVLA on real-world robots.

## 1. Introduction

Vision-Language-Action (VLA) models are moving embodied intelligence toward generalization by injecting semantic

<sup>\*</sup>Equal contribution <sup>1</sup>University of Science and Technology of China, Hefei, China. Correspondence to: Jianmin Ji <jianmin@ustc.edu.cn>, Yanyong Zhang <yanyongz@ustc.edu.cn>.

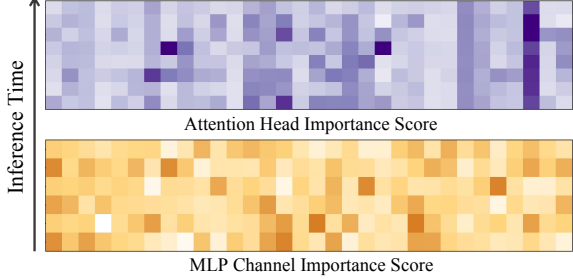


Figure 1. During VLA execution, channel importance scores vary dynamically as the environment evolves, causing the optimal sparsity pattern to shift accordingly.

understanding into robot control (Black et al.; Li et al., 2024a; Kim et al., 2024). Despite promising real-world results from recent VLA models such as OpenVLA (Kim et al., 2024) and  $\pi_{0.5}$  (Intelligence et al.), inference latency remains the primary bottleneck for real-time control (Yang et al., 2025). In this context, token pruning (Wang et al., 2025; Liu et al., 2025) has been extensively researched as a method to reduce input size, which decreases latency by discarding redundant visual tokens at the risk of losing critical semantics with high pruning ratio. While token-level optimization has been thoroughly studied (Shinde et al., 2025), comparatively little attention has been paid to VLA model pruning. In this work, we focus on VLA model pruning, an area with less research, to further accelerate inference by reducing redundant model parameters. Typically, a VLA architecture comprises a lightweight action expert and a heavy VLM backbone, which dominates the parameter count and shows high sparsity, making it a prime target for pruning (Chen & Li, 2025; Jabbour et al., 2025).

Existing research on VLA model sparsification primarily bifurcates into two directions, static and dynamic pruning. Static pruning, such as RLRC (Chen & Li, 2025) and GLUE-STICK (Jabbour et al., 2025), prunes parameters based on fixed calibration data. However, they fail to adapt to the dynamic evolving task environment (e.g., transitioning from large-scale navigation to fine-grained local manipulation) where optimal sparsity patterns vary dynamically, as shown in Fig.1 (Liu et al., 2023b). Consequently, these static approaches often suffer performance degradation under dy-

namic sparsity shifts. Moreover, they are heavily shackled by the requirement for massive retraining cycles or a reconstruction process that incurs unsustainable computational costs. To address the inflexibility of static approaches, dynamic pruning like MoLe-VLA (Zhang et al., 2025) and DeeR-VLA (Yue et al., 2024) selects layers at fixed intervals based on runtime inputs but suffer from critical drawbacks: the dependency on auxiliary routers incurs extra training and runtime inference overheads, while their coarse layer-level granularity overlooks fine-grained intra-layer redundancy.

To bridge these gaps, a training-free, fine-grained, and environment-aware adaptive model pruning method is urgently needed. However, two major challenges remain. First, VLA models’ sparsity patterns evolve with the environment, making real-time computation difficult. Additionally, relying only on instantaneous observations fails to capture the continuous nature of VLA execution. Second, adaptive pruning introduces real-time overhead. While existing methods for LLMs use large-batch inference to amortize overhead across multiple samples (Le et al., 2025), VLA models constrained by single-sample streaming bear the pruning overhead individually, directly adding it to the end-to-end inference latency. For frequency-sensitive VLA models, such delays limit the effective policy update rate, inducing robotic stuttering and jittering (Black et al., 2025).

To address these challenges, we propose **EcoVLA**, a training-free, plug-and-play pruning framework capable of adapting sparsity patterns via real-time environmental perception while minimizing pruning overhead through non-blocking parallel inference. EcoVLA comprises two core components: **Environment-aware Adaptive Pruning (EAP)** and **Interleaved Inference Orchestration (I<sup>2</sup>O)**.

EAP is a lightweight, environment-aware adaptive structured channel pruning method. First, leveraging visual observations, EAP perceives environmental dynamics to identify variations in sparsity patterns. Crucially, to maintain the temporal consistency essential for stable VLA execution, we incorporate a temporal feature aggregation strategy. By strategically integrating the instantaneous features with historical features, EAP precisely identifies redundant channels for pruning. The continuous update of historical features with the latest features further guarantees the temporal consistency of the sparsity patterns.

I<sup>2</sup>O replaces the conventional sequential paradigm with a non-blocking parallel paradigm, strategically exploiting FLOPs Bubbles within VLA inference. Specifically, I<sup>2</sup>O orchestrates two parallel streams, comprising an Inference Stream for real-time action generations and a Pruning Stream for pruning execution. By interleaving pruning computations into the FLOPs bubbles, we maximize overall hardware utilization, effectively masking the pruning overhead to ensure robust real-time streaming control. We

evaluate EcoVLA on robotic manipulation across two simulators (LIBERO (Liu et al., 2023a) and SIMPLER (Sun et al., 2023)) and three VLA models (OpenVLA-OFT (Kim et al., 2025),  $\pi_{0.5}$  (Intelligence et al.) and CogACT (Li et al., 2024a)). EcoVLA achieves  $1.6\times$  speedup with only a 0.4% reduction in success rate. Furthermore, by integrating with token pruning methods, EcoVLA boosts the speedup from  $1.21\times$  (achieved by FastV with a 50% pruning ratio) to  $2.18\times$ . Crucially, it recovers the accuracy drop caused by FastV, narrowing the performance gap with the vanilla baseline to just 0.5%. To validate our approach beyond simulation, we deploy EcoVLA on a 7-DoF Kinova Gen3 robot, demonstrating its practical acceleration capabilities in real-world scenarios.

## 2. Related Work

**Vision-Language-Action Models.** VLAs extend VLMs by incorporating action modalities for embodied control (Brohan et al., 2022; Black et al.). Despite their efficacy, deployment is constrained by high computational costs (Yang et al., 2025). As action heads (e.g., MLPs, diffusion) are lightweight, the VLM backbone remains the dominant computational bottleneck (Zhang et al., 2025; Ma et al., 2025).

**Efficient Vision-Language-Action Models.** VLA acceleration typically employs token pruning (Wang et al., 2025; Liu et al., 2025) or KV caching (Xu et al., 2025) to exploit input redundancy. Regarding model sparsification, static methods (Chen & Li, 2025; Jabbour et al., 2025) prune parameters offline but lack environmental adaptability and require retraining. Conversely, fixed-interval dynamic methods (Yue et al., 2024; Zhang et al., 2025) offer task-dependence but suffer from high retraining costs and limited transferability. Consequently, a training-free, plug-and-play, and fine-grained adaptive pruning framework is needed.

## 3. Preliminaries

### 3.1. Vision-Language-Action Models

Vision-Language-Action (VLA) models unify visual and linguistic inputs to generate robotic actions, typically consisting of a Vision-Language Model (VLM) backbone and an Action Expert (Kim et al., 2025; Wen et al., 2025). While Action Expert architectures vary (e.g., Diffusion-based or Parallel Decoding) (Kim et al., 2025), they are lightweight compared to the VLM backbone. Thus, the VLM constitutes the primary bottleneck, rendering its standardized architecture the ideal candidate for pruning.

### 3.2. Formulation of VLA Structured Pruning

Let  $\pi_\Theta$  be a VLA model with Large Language Model (LLM) backbone  $\Theta$ . We target  $\Theta$  for pruning due to its domi-

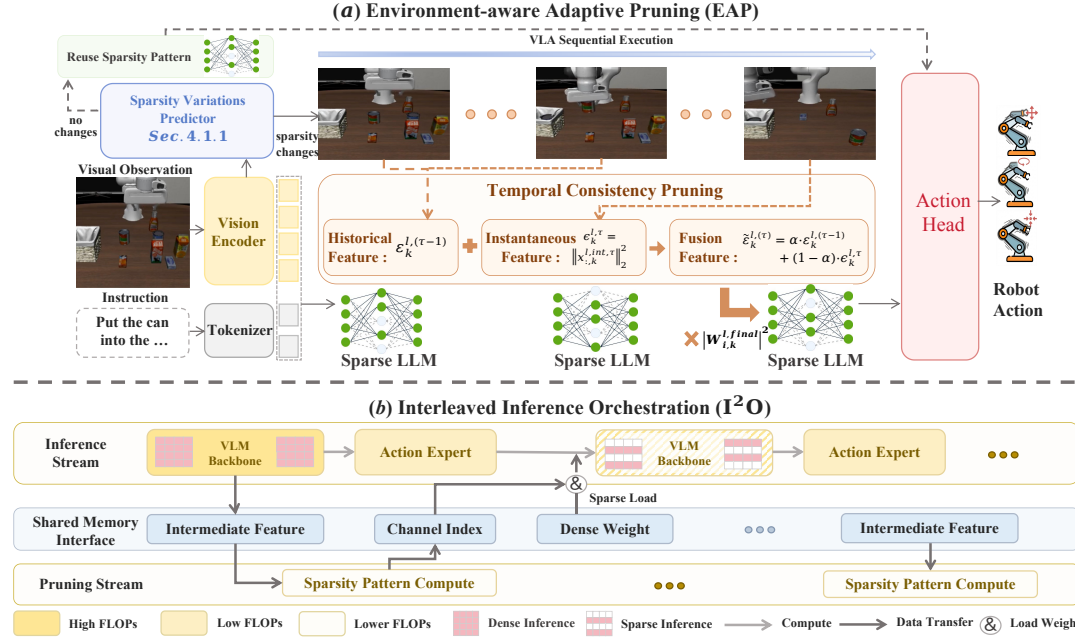


Figure 2. Overall pipeline of EcoVLA. (a) Environment-aware Adaptive Pruning (EAP): EAP is a lightweight, environment-aware method that identifies sparsity variations by perceiving real-time dynamics. Considering the temporal consistency of VLA execution in physical environments, EAP integrates instantaneous features with historical features to jointly compute the sparsity pattern. (b) Interleaved Inference Orchestration ( $I^2O$ ):  $I^2O$  interleaves sparsity pattern computation into the inherent FLOPs bubbles within the VLA inference using a non-blocking parallel paradigm.

nant model size. We optimize a structural binary mask  $\mathbf{m} \in \{0, 1\}^{|\Theta|}$  (where grouped elements share values) to minimize the divergence between dense and pruned policies:

$$\arg \min_{\mathbf{m}} \mathcal{L}(\pi_{\Theta}, \pi_{\Theta \odot \mathbf{m}}, \mathcal{D}) \quad \text{s.t.} \quad \|\mathbf{m}\|_0 = \kappa \quad (1)$$

where  $\odot$  denotes the element-wise product,  $\kappa$  is sparsity constraint,  $\mathcal{D}$  represents the calibration dataset. The objective  $\mathcal{L}$  measures the divergence between models.

To efficiently solve the global optimization problem defined in (1), we decompose the LLM into layer-wise reconstruction paradigm (An et al., 2024; Le et al., 2025). The LLM consists of  $L$  blocks. Each block  $l$  transforms the input hidden state  $\mathbf{X}^l \in \mathbb{R}^{B \times S \times D}$  via a residual mapping:

$$\mathbf{X}^{l+1} = \mathbf{X}^l + \mathcal{F}^l(\mathbf{X}^l) \quad (2)$$

We decompose the block function  $\mathcal{F}^l$  into an intermediate transformation and a final linear projection:

$$\mathcal{F}^l(\mathbf{X}^l) = \mathbf{X}^{l,\text{int}}(\mathbf{W}^{l,\text{final}})^T, \quad \mathbf{X}^{l,\text{int}} = \mathcal{T}^l(\text{LN}(\mathbf{X}^l)) \quad (3)$$

Here,  $\mathcal{T}^l$  is intermediate transformations (e.g.,  $\mathbf{W}^K$  or  $\mathbf{W}^{\text{up}}$ ), while  $\mathbf{W}^{l,\text{final}}$  represents the final weight matrix (e.g.,  $\mathbf{W}^O$  or  $\mathbf{W}^{\text{down}}$ ). For hardware acceleration, structured pruning aligns output channels with input channels, retaining indices  $\mathbb{C}^l \subseteq \{1, 2, \dots, C_{\text{in}}\}$ :

$$\begin{aligned} \widetilde{\mathbf{W}}^{l,\text{gate}} &= \mathbf{W}^{l,\text{gate}}[\mathbb{C}^l, :], & \widetilde{\mathbf{W}}^{l,\text{up}} &= \mathbf{W}^{l,\text{up}}[\mathbb{C}^l, :], \\ \widetilde{\mathbf{W}}^{l,\text{down}} &= \mathbf{W}^{l,\text{down}}[:, \mathbb{C}^l], \end{aligned} \quad (4)$$

where  $\widetilde{\mathbf{W}}^{l,\text{gate}}, \widetilde{\mathbf{W}}^{l,\text{up}} \in \mathbb{R}^{|\mathbb{C}^l| \times C_{\text{out}}}$  and  $\widetilde{\mathbf{W}}^{l,\text{down}} \in \mathbb{R}^{C_{\text{out}} \times |\mathbb{C}^l|}$ . The notation  $|\mathbb{C}^l|$  is the cardinality of  $\mathbb{C}^l$ . Similarly, in attention blocks, pruning heads removes coupled output channels of  $\mathbf{W}^{Q,K,V}$  and input channels of  $\mathbf{W}^O$ .

## 4. Methodology

In this section, we introduce EcoVLA, the first training-free, plug-and-play adaptive pruning framework for VLA models, as illustrated in Fig.2. We first detail Environment-aware Adaptive Pruning (EAP) in Sec.4.1, which begins with a lightweight predictor to identify real-time sparsity variations and subsequently employs a pruning method based on temporal consistency. Next, we introduce Interleaved Inference Orchestration ( $I^2O$ ) in Sec.4.2, a parallel execution paradigm that exploits inference FLOPs bubbles to schedule pruning operations, thereby reducing additional overhead.

### 4.1. Environment-aware Adaptive Pruning

#### 4.1.1. LIGHTWEIGHT ENVIRONMENT-AWARE SPARSITY VARIATIONS PREDICTOR

The optimal sparsity patterns of VLA models evolve dynamically during execution. To capture these changes efficiently, we introduce a lightweight environment aware sparsity variations predictor. This module leverages visual feature similarities alongside a temporal context-conditioned trigger, enabling rapid and robust identification of changes.

**Lightweight Visual Similarity Metric.** To avoid introducing substantial computational overhead, we discard the popular attention-based semantic similarity (Xu et al., 2025), opting instead to leverage the visual features extracted by the VLA visual encoder to compute the similarity between step  $t$  and  $t - 1$ . Let  $f_t, f_{t-1} \in \mathbb{R}^{N \times D}$  denote the image token features, where  $N$  is the number of visual tokens and  $D$  is the feature dimension. We define the similarity score as the average token-wise cosine similarity:

$$s_t = \frac{1}{N} \sum_{i=1}^N \frac{f_t^i \cdot f_{t-1}^i}{\|f_t^i\|_2 \|f_{t-1}^i\|_2} \quad (5)$$

We posit that if the visual features  $f_t$  and  $f_{t-1}$  exhibit high similarity, the sparsity pattern remains stable between frames. Conversely, significant deviation in visual features implies considerable variation in the sparsity pattern.

**Temporal Context-Conditioned Sparsity Trigger.** In open-world robotic manipulation, the environment is dynamic, causing the distribution of visual feature similarities to evolve over time. Since we rely on these similarities to update sparsity pattern, a static decision criterion becomes brittle under distribution shifts. Therefore, we introduce a lightweight Temporal Context-Conditioned Sparsity Trigger, which leverages temporal context to adapt to such shifts. Specifically, we maintain a fixed-size sliding window  $\mathcal{H}_t$  storing the similarities of the recent  $T$  frames:

$$\mathcal{H}_t = \{s_{t-T}, s_{t-T+1}, \dots, s_{t-1}\} \quad (6)$$

Based on this temporal context, we adopt a dynamic decision criterion where the sparsity update is triggered if the current similarity drops below the  $p$ -th quantile of the  $\mathcal{H}_t$ . The sparsity pattern update policy is formally defined as:

$$u_t = \mathbb{I}(s_t < \text{Quantile}(\mathcal{H}_t, p)) \quad (7)$$

Here,  $p$  serves as a sensitivity hyperparameter, where a higher  $p$  enhances responsiveness to subtle changes, whereas lower  $p$  prioritizes stability. This mechanism yields self-regulative behavior. During rapid motion, the quantile naturally decreases, suppressing excessive updates to ensure stability. Conversely, in stable phases, the quantile increases, facilitating the sensitive detection of fine-grained variations.

#### 4.1.2. TEMPORAL CONSISTENCY PRUNING

This section details the sparsity pattern computation. Upon triggering a sparsity update at frame  $t$ , we execute a dense inference to perform the pruning calculation. We first compute the instantaneous features from the current input at frame  $t$ , which are subsequently aggregated with historical features. The newly computed sparsity pattern is then applied starting from the frame  $t + 1$  for sparse inference.

To formalize this computation, we denote the update triggered at frame  $t$  as the  $\tau$ -th sparsity update step. Specifically, as the current input reaches block  $l$ , following the

formulation in Sec.3.2, we can compute the current intermediate hidden states  $\mathbf{X}^{l,\text{int},\tau} = \mathcal{T}^l(\text{LN}(\mathbf{X}^{l,\tau}))$ . Given that VLA models operate on single-sample streaming inputs, the dimensionality of  $\mathbf{X}^{l,\text{int},\tau}$  is defined as  $(1, S, C_{in})$ . For notational simplicity, we omit the batch dimension in the subsequent formulation. To quantify the activation of the current input across structured channels, we compress the activation along the sequence dimension to obtain the instantaneous feature. Formally, for the  $k$ -th structured channel, the calculation is performed as follows:

$$\epsilon_k^{l,\tau} = \sum_{j=1}^S \left( \mathbf{X}_{j,k}^{l,\text{int},\tau} \right)^2 = \left\| \mathbf{X}_{:,k}^{l,\text{int},\tau} \right\|_2^2 \quad (8)$$

where  $\epsilon_k^{l,\tau}$  represents the instantaneous feature of the  $k$ -th structured channel given the current input.

However, relying solely on instantaneous features is sub-optimal, as the physical execution of VLA models exhibits inherent temporal consistency. This temporal consistency is characterized by smooth, continuous transitions in both physical environments and proprioceptive states across adjacent frames, rather than discrete, abrupt jumps. In light of this, we aggregate the instantaneous feature with the historical feature. Specifically, we initialize the historical feature  $\mathcal{E}^{l,(0)} \in \mathbb{R}^{C_{in}}$  for each block  $l$  by applying Eq. 8 on a calibration dataset. For each subsequent update step  $\tau$ , we can compute the fused feature by leveraging the previous historical feature  $\mathcal{E}^{l,(\tau-1)}$  as a temporal prior:

$$\tilde{\mathcal{E}}_k^{l,\tau} = \alpha \cdot \mathcal{E}_k^{l,(\tau-1)} + (1 - \alpha) \cdot \epsilon_k^{l,\tau} \quad (9)$$

where  $\alpha \in [0, 1]$  is the temporal inertia parameter. A larger  $\alpha$  leads to a more conservative update. We update the historical feature on full channels using an exponential moving average. Here, the momentum  $\lambda$  ensures temporal consistency, providing a stable prior for subsequent steps:

$$\mathcal{E}^{l,\tau} = \lambda \cdot \mathcal{E}^{l,(\tau-1)} + (1 - \lambda) \cdot \tilde{\mathcal{E}}_k^{l,\tau} \quad (10)$$

Finally, we can compute the sparsity pattern. Following PPsp (Le et al., 2025), we evaluate the significance of the  $k$ -th channel in the  $l$ -th layer based on both weight magnitude and fused feature. Let  $\mathbf{W}^{l,\text{final}} \in \mathbb{R}^{C_{out} \times C_{in}}$  denote the final weight matrix in block  $l$ . The importance score  $\mathcal{S}_k^{l,\tau}$  is formulated as:

$$\mathcal{S}_k^{l,\tau} = \left\| \left\{ \left| W_{i,k}^{l,\text{final}} \right|^2 \cdot \tilde{\mathcal{E}}_k^{l,\tau} \right\}_{i=0}^{C_{out}} \right\|_2 \quad (11)$$

where  $\{\cdot\}$  denotes the set of elements, and  $\mathcal{S}^{l,\tau} \in \mathbb{R}^{C_{in}}$ . Crucially, identifying and pruning the  $k$ -th input channel of  $\mathbf{W}^{l,\text{final}}$  (associated with low  $\mathcal{S}_k^{l,\tau}$ ) necessitates the simultaneous removal of the corresponding  $k$ -th output channel of the intermediate transformations  $\mathcal{T}^l$ .

#### 4.1.3. ANALYSIS OF COMPUTATIONAL COST

The computational overhead of EAP is primarily divided into visual feature similarity and sparsity pattern computation. For an image represented by  $N$  visual tokens with feature dimension  $D$  and a block with  $C_{in}$  input and  $C_{out}$  output channels, the sparsity pattern overhead includes instantaneous feature computation, feature fusion, historical feature updates for  $C_{in}$  channels, and importance score computation. Although weight  $L_2$ -norms are typically pre-computed to reduce online costs to  $1 \cdot C_{in}$ , the worst-case complexity occurs when weight magnitudes are computed online, leading to the following FLOPs formulation:

$$\text{FLOPs} \approx 5ND + 2SC_{in} + 3C_{in}C_{out} + 4C_{in} \quad (12)$$

The computational overhead of EAP is marginal, as it primarily consists of element-wise operations that exhibit a negligible footprint compared to the VLA.

### 4.2. Interleaved Inference Orchestration

In this section, we first analyze the computational characteristics of VLA inference, revealing FLOPs bubbles arising from resource under-utilization. We then introduce **Interleaved Inference Orchestration (I<sup>2</sup>O)**, which exploits the complementary resource profiles between the VLM Backbone and Action Expert stages to absorb sparsity pattern computation into these bubbles with minimal overhead (Fig.2). Finally, we present hardware-efficient implementations to further accelerate both dense and sparse execution.

#### 4.2.1. FLOPS BUBBLES OF VLA INFERENCE

In this section, our profiling reveals temporal FLOPs bubbles during VLA inference due to a mismatch between model workload and hardware capacity, providing an opportunity to absorb sparsity pattern computation overhead.

**The VLM Backbone Stage.** This stage is dominated by large-scale General Matrix Multiplications (GEMMs) within the transformer layers, rendering it inherently compute-bound. Given the massive model dimensions ( $N, K$ ) and the extensive sequence length ( $M$ ), the arithmetic intensity ( $I$ ) of these operations significantly exceeds the hardware's compute-to-memory ratio:

$$\frac{\text{FLOPs}}{\text{Bytes}} = \frac{2 \cdot M \cdot N \cdot K}{2 \cdot (NK + MK + MN)} \gg \frac{T_{\text{compute}}}{T_{\text{bandwidth}}} \quad (13)$$

where  $T_{\text{compute}}$  and  $T_{\text{bandwidth}}$  compute throughput and memory bandwidth, respectively. Consequently, the GPU Tensor Cores operate at near-peak saturation, while the memory bandwidth remains largely under-saturated, providing the necessary headroom for concurrent auxiliary tasks.

**The Action Expert Stage.** In stark contrast, this stage consists of lightweight MLPs or diffusion-based denoising

steps. Operating under the real-time, robotic control streaming (batch size = 1), computational demand falls orders of magnitude below the GPU's peak parallel processing capacity. In this state, the powerful Tensor Cores remain largely under-utilized, leaving a substantial computational reservoir that can be reclaimed to execute auxiliary tasks.

#### 4.2.2. HIDING PRUNING OVERHEADS VIA I<sup>2</sup>O

The conventional synchronous pruning stream is serially scheduled either preceding or succeeding the main inference stream, thereby linearly increasing the total latency. To circumvent this bottleneck, EcoVLA introduces **Interleaved Inference Orchestration (I<sup>2</sup>O)** as illustrated in Fig.2, whose core philosophy is to interleave sparsity pattern computation into the FLOPs bubbles of the VLA pipelines.

Specifically, we decouple the sparsity pattern computation for step  $t + 1$  from the main dense inference of the current step  $t$  by dispatching it to a parallel pruning stream. During the VLM Backbone stage, where the GPU is compute-saturated but memory bandwidth remains undersaturated, the pruning stream concurrently buffers the requisite intermediate activations. Subsequently, as the inference transitions to the Action Expert stage, I<sup>2</sup>O interleaves the sparsity pattern computation into FLOPs bubbles, effectively utilizing the idle Tensor Cores. As a result, I<sup>2</sup>O fully taps into the GPU's untapped computational potential, achieving a balanced workload distribution across the inference pipeline. By interleaving the sparsity pattern computation into the FLOPs bubbles, our approach avoids intense GPU resource contention, enabling low latency sparsity pattern computation overhead.

Building on this efficient orchestration, we now turn our attention to the latency analysis of I<sup>2</sup>O. Let  $T_{\text{infer}}$  denote the VLA inference latency and  $T_{\text{prune}}$  the overhead. In conventional synchronous approaches, the total latency is additive:  $L_{\text{synch}} = T_{\text{infer}} + T_{\text{prune}}$ . In I<sup>2</sup>O, the latency becomes  $L_{I^2O} = T_{\text{infer}} + \delta$ , where  $\delta$  accounts for the overhead induced by concurrent execution, such as Streaming Multiprocessor (SM) scheduling costs, memory bandwidth contention and minor GPU resource competition. Owing to the lightweight design of the adaptive pruning module and its execution within FLOPs bubbles,  $\delta$  is minimal. Consequently, this orchestration ensures that adaptive pruning is integrated seamlessly without impacting the latency-sensitive VLA control loop, thus maintaining the high-frequency reactivity essential for smooth robotic manipulation.

### 4.3. Hardware-efficient Implementation

In this section, we detail the hardware-level optimizations implemented for both dense and sparse VLA inference to achieve practical inference acceleration.

#### 4.3.1. SPARSE EFFICIENT KERNELS

We apply three kernel-level optimizations targeting memory efficiency and computation throughput in sparse inference.

**Sparse Linear Transformation Kernel.** In the standard PyTorch implementation, the retained weights are indexed before performing the linear transformation, which incurs additional memory I/O overhead. In contrast, we have implemented a sparse linear transformation Triton kernel that directly loads only the retained weights during computation, avoiding this overhead and improving efficiency.

**Memory coalescing.** As described in Sec.3.2, when performing pruning on the  $W_{\text{down}}$  weights of the MLP, we actually prune the columns of the weights. In the sparse implementation, this results in indices pointing to non-contiguous memory regions, leading to reduced memory access efficiency. We simply store these matrices in column-major format to enhance memory access locality. Similarly, we also store the output projection weights  $W_O$  in the self-attention module in a column-major format.

**High-Performance Fused Kernels.** During sparse VLA inference, the MLP computes gate projection, up projection, SiLU activation, and element-wise multiplication. We fuse these four operations into a single Triton kernel that reads the input once and keeps intermediate results in registers, eliminating redundant memory traffic and reducing kernel launches from 4 to 1, yielding nearly  $2\times$  speedup in practice.

#### 4.3.2. DENSE METRIC ACCELERATION

In addition to I<sup>2</sup>O, we apply two memory-level optimizations to accelerate sparsity pattern computation.

**Allocation-Free Caching.** As noted in Eq.11, computing the sparsity pattern involves weight norms and activation norms, where standard implementations suffer from repeated weight loading and dynamic memory allocation. We address this by pre-computing weight norms as compact vectors (a 99.97% reduction) and pre-allocating static activation buffers, transforming memory-bound operations into lightweight lookups while eliminating runtime allocations.

**Batched Metric Computation.** Per-layer sparsity computation incurs many separate kernel launches. We instead stack weight norms and activation buffers across layers into contiguous tensors, enabling kernel fusion that amortizes launch overhead and exposes layer-level parallelism.

## 5. Experiments

### 5.1. Experimental Settings

**Baselines.** To validate the generalizability of EcoVLA, we evaluate it across diverse VLA architectures. In simulation, we conduct experiments on open-source VLA models,

including OpenVLA-OFT (Kim et al., 2025),  $\pi_{0.5}$  (Intelligence et al.), and CogACT (Li et al., 2024a). For fair comparison, we benchmark EcoVLA against Wanda (Sun et al., 2023), a mainstream static pruning method. Beyond standalone improvements, we demonstrate that EcoVLA is broadly compatible and can be stacked with other acceleration techniques. Experiments combining EcoVLA with FastV (Chen et al., 2024) and VLA-Cache (Xu et al., 2025) yield substantial additional speedups with negligible performance degradation. For real-world evaluation, we fine-tune  $\pi_{0.5}$  for deployment on a 7-DoF Kinova Gen3 robotic arm. The model is trained for 10,000 steps with default parameters. See App.A for further details.

**Evaluation Protocol.** To ensure a comprehensive comparison, we adopt different pruning ratios. Specifically, for OpenVLA-OFT (Kim et al., 2025) and CogACT (Li et al., 2024a), we perform evaluations at pruning ratios of 25% and 40%, while for  $\pi_{0.5}$  (Intelligence et al.), we evaluate at 25% and 37.5% to accommodate the architecture. The evaluation metrics primarily include task success rate(%), inference latency( $ms$ ), and FLOPs( $T$ ).

**Implementation Details.** We follow the original experimental settings of FastV (Chen et al., 2024) and VLA-Cache (Xu et al., 2025). All experiments conducted on an NVIDIA RTX 3090 GPU, and latency is measured following VLA-Cache. Since VLA-Cache is incompatible with FlashAttention (Dao et al., 2022), we use eager LlamaAttention when integrating EcoVLA with VLA-Cache; otherwise, FlashAttention is enabled by default. More hyperparameter details are provided in the App.A.3.

**Benchmarks.** We evaluate EcoVLA on two simulators and three real-robot tasks. The LIBERO (Liu et al., 2023a) benchmark is designed to evaluate robotic manipulation capabilities across four task suites: LIBERO-Spatial, LIBERO-Object, LIBERO-Goal, and LIBERO-Long. Each task suite examines different capabilities of VLA. The SIMPLER (Li et al., 2024b) simulation environment provides two evaluation settings, including Visual Matching and Variant Aggregation. We evaluate four tasks on the Google Robot arm: 1) *Pick Coke Can (PickCan)*, 2) *Move Near (MoveNear)*, 3) *Open/Close Drawer (Drawer)*, and 4) *Open Top Drawer and Place Apple (DrawerApple)*. To assess EcoVLA in real-world settings, we conduct experiments across three tasks (shown in Fig.3): *Place the apple in the basket*, *Put the pill bottle in the cabinet*, and *Place the banana in the basket*. More details are provided in the App.A.4.

### 5.2. Main Results

**Results on OpenVLA-OFT.** Using the LIBERO benchmark, we evaluate EcoVLA on OpenVLA-OFT and show its compatibility by combining it orthogonally with acceleration techniques like FastV and VLA-Cache. Tab.1

Table 1. Performance of EcoVLA on OpenVLA-OFT in LIBERO at 25% and 40% pruning ratio.

Method	Success Rate (%) ↑					FLOPs (T) ↓	Latency (ms) ↓	Speedup ↑
	LIBERO-Spatial	LIBERO-Object	LIBERO-Goal	LIBERO-Long	Average			
<i>Pruning Ratio 25%</i>								
Vanilla	97.6	98.4	96.2	94.6	96.7	4.05 (100.0%)	143.56 (162.78)	1.00×
FastV	96.4	97.2	89.0	94.8	94.4	2.49 (61.48%)	118.57	1.21×
VLA-Cache	96.6	98.6	96.4	94.8	96.6	3.03 (74.81%)	148.51	1.10×
<i>Pruning Ratio 40%</i>								
Wanda	95.8	98.8	87.2	93.2	93.8	3.14 (77.53%)	124.32	1.15×
<b>Ours</b>	97.4	98.8	94.6	96.4	96.8	3.23 (79.75%)	113.98	1.26×
<b>FastV + Ours</b>	96.6	98.2	94.0	96.0	96.2	1.96 (48.39%)	65.85	2.18×
<b>VLA-Cache + Ours</b>	96.8	98.4	92.4	94.2	95.5	2.43 (60.00%)	121.24	1.34×

 Table 2. Performance of EcoVLA on  $\pi_{0.5}$  in LIBERO at 25% and 37.5% pruning ratio.

Method	Sparsity	Success Rate (%) ↑					FLOPs (T) ↓	Latency (ms) ↓	Speedup ↑
		LIBERO-Spatial	LIBERO-Object	LIBERO-Goal	LIBERO-Long	Average			
Vanilla	0%	98.8	98.2	98.0	92.4	96.9	1.99 (100.0%)	81.94	1.00×
<b>Ours</b>	25.0%	98.2	98.6	98.4	91.6	96.7	1.64 (82.41%)	62.66	1.31×
	37.5%	97.8	98.4	96.8	87.0	95.0	1.47 (73.87%)	55.98	1.46×

Table 3. Performance of EcoVLA on CogACT in SIMPLER at 25% and 40% pruning ratio.

SIMPLER	Method	Sparsity	Success Rate (%) ↑					FLOPs(T)↓	Latency (ms) ↓	Speedup ↑
			Pick Coke	Move Near	Open/Close	Open Top	Average			
Visual Matching	Vanilla	0	93.3	83.8	74.5	41.7	73.3	1.81 (100.0%)	104.16	1.00×
	<b>ours</b>	25%	95.0	82.1	70.8	38.9	71.7	1.45 (80.11%)	72.65	1.44×
	<b>ours</b>	40%	93.0	85.4	73.5	42.6	73.6	1.25 (69.06%)	66.43	1.57×
Variant Aggregation	Vanilla	0	88.7	76.8	26.7	51.9	61.0	1.81 (100.0%)	105.87	1.00×
	<b>ours</b>	25%	85.9	75.3	27.2	46.0	58.6	1.47 (81.22%)	73.98	1.43×
	<b>ours</b>	40%	86.1	74.3	33.1	48.7	60.6	1.28 (70.72%)	66.25	1.60×

 Table 4. Performance of EcoVLA on  $\pi_{0.5}$  on a real-world robot.

Method	Task1	Task2	Task3	Latency(ms)
baseline	12/20	18/20	16/20	86.08
Ours	12/20	16/20	15/20	68.40



Figure 3. Robot Manipulation on Kinova Gen3 Platform.

shows that EcoVLA achieves 1.26× and 1.41× speedups at 25% and 40% pruning ratios, with success rate losses of only 0.35% and 2.8%, respectively. The robustness of EcoVLA is particularly pronounced on the pruning-sensitive LIBERO-Goal benchmark, significantly outperforming the mainstream method Wanda. Specifically, EcoVLA establishes a commanding lead of 7.4% and 12.4% over Wanda at the respective pruning ratios. Beyond this robustness, EcoVLA achieves lower latency than Wanda despite a additional pruning overhead, as I<sup>2</sup>O conceals the pruning

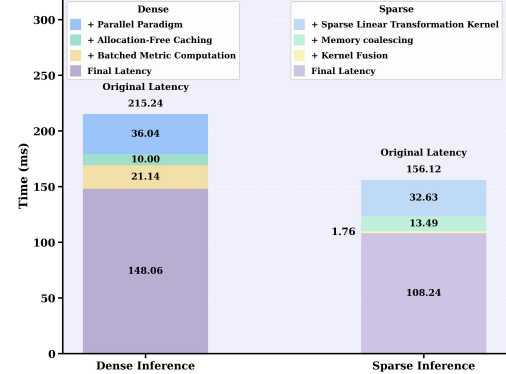


Figure 4. Acceleration breakdown for dense and sparse inference.

cost within FLOPs bubbles. Combined with our hardware-efficient design, this enables EcoVLA to deliver distinctly higher wall-clock speedups over Wanda.

Our results empirically validate the broad compatibility of EcoVLA. When combined with FastV (50% token pruning), it achieves a 2.18× speedup with a negligible 0.5% loss at 25% sparsity, and reaches a 2.35× speedup at 40%. When combined with VLA-cache, it achieves a 1.34× speedup with a negligible 0.5% loss at 25% sparsity, and reaches a

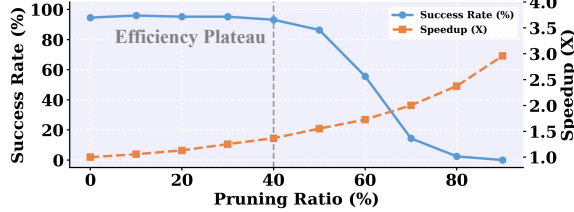


Figure 5. Trade-off between Success Rate and Latency.

Table 5. Overhead of Pruning Stream.

Execution Method	Latency (ms)
Normal VLA Inference	143.56
$I^2O$	148.06

$2.35\times$  speedup at 40%. Notably, these combinations deliver significantly higher speedups compared to the standalone baselines. While generally incurring only a slight decline in success rate, intriguingly, we observe a performance improvement in the FastV combination. We attribute this phenomenon to the regularization effect induced by our precise, adaptive model sparsification (Jin et al., 2022).

**Results on  $\pi_{0.5}$ .** To demonstrate the cross-model generalizability of EcoVLA, we conduct experiments on the state-of-the-art VLA model,  $\pi_{0.5}$ , as shown in Tab.2. At 25% and 37.5% pruning ratios, EcoVLA achieves  $1.31\times$  and  $1.46\times$  speedups with marginal accuracy drops of 0.2% and 1.85%, respectively. Notably, for the LIBERO-Object, we observe a 0.2% accuracy improvement at the 37.5% pruning ratio. This observation corroborates the regularization benefit discussed earlier, suggesting that selective pruning effectively filters out noise from redundant parameters. Most significantly, despite  $\pi_{0.5}$ 's inherently efficient structure and low latency (81.94 ms), EcoVLA still manages to extract a substantial  $1.46\times$  acceleration. This capability to further accelerate an already fast model redefines the standards for efficient real-time deployment.

**Results on CogACT.** We evaluate EcoVLA's generalization on CogACT within SIMPLER, as summarized in Tab.3. In the Visual Matching setting, EcoVLA achieves a  $1.57\times$  speedup at a 40% pruning ratio with a success rate drop of only 0.3%. Similarly, in the Variant Aggregation setting, it reaches a  $1.6\times$  speedup at 40% pruning while incurring a marginal accuracy reduction of 0.6%.

**Results on Real Robot.** We evaluate real-world performance on a physical 7-DoF Kinova Gen3 arm controlled by  $\pi_{0.5}$ . As shown in Tab.3, our approach delivers a  $1.26\times$  wall-clock speedup at the cost of minor performance loss, underscoring its viability for real-robot deployment. We further analyze the underlying reasons in App.B.

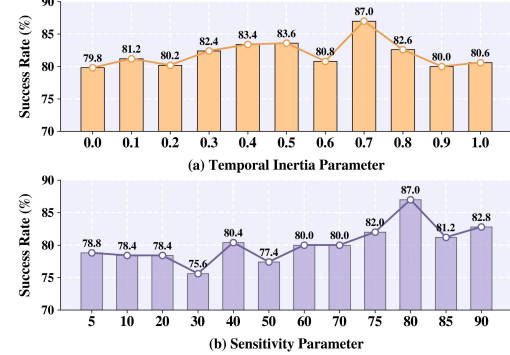


Figure 6. Impact on Hyperparameters  $\alpha$  and  $p$ .

### 5.3. More Results

**Ablation Study on Acceleration.** Fig.4 details the acceleration breakdown. For dense inference, bubble scheduling, buffer optimization, and batched metrics reduce latency by 36.04 ms, 10 ms, and 21.14 ms respectively, yielding 148.06 ms. For sparse inference, utilizing sparse kernels, memory coalescing, and kernel fusion cuts latency by 36.04 ms, 13.49 ms, and 1.76 ms, resulting in 108.24 ms.

**Trade-off between Performance and Latency.** As shown in Fig.5, we analyze the trade-off between success rate and latency. While the success rate remains robust below 40% pruning, it deteriorates rapidly beyond this threshold. We observe an optimal trade-off between performance and latency at a 40% pruning ratio.

**Overhead of Pruning Stream.** The parallel pruning stream introduces overhead  $\delta$  (e.g., SM scheduling), detailed in Tab.5. Due to the lightweight design,  $\delta$  is limited to 4.5 ms.

**Hyperparameters Studies.** Fig.6 analyzes the impact of  $\alpha$  and  $p$  on LIBERO-Long. High  $\alpha$  over-reliance on historical features, causing sparsity lag, while low  $\alpha$  leads to instability. Performance peaks at  $\alpha = 0.7$ , validating our design. Similarly, low  $p$  overlooks subtle cues, whereas high  $p$  causes hypersensitivity to noise. The peak success rate at  $p = 80\%$  confirms EcoVLA effectively filters noise while maintaining the sensitivity required for robust operation. Additional analysis is provided in the App.C

## 6. Conclusion

We present EcoVLA, a training-free, plug-and-play adaptive pruning framework for VLA models that combines Environment-aware Adaptive Pruning (EAP) with Interleaved Inference Orchestration ( $I^2O$ ) to update sparsity online with negligible overhead. We validate EcoVLA on both real robots and high-fidelity simulators.

## References

An, Y., Zhao, X., Yu, T., Tang, M., and Wang, J. Fluctuation-based adaptive structured pruning for large language models. In *Proceedings of the AAAI Conference on Artificial Intelligence*, volume 38, pp. 10865–10873, 2024.

Black, K., Brown, N., Driess, D., Esmail, A., Equi, M., Finn, C., Fusai, N., Groom, L., Hausman, K., Ichter, B., et al.  $\pi 0$ : A vision-language-action flow model for general robot control. *corr, abs/2410.24164*, 2024. doi: 10.48550. *arXiv preprint ARXIV.2410.24164*.

Black, K., Galliker, M. Y., and Levine, S. Real-time execution of action chunking flow policies. *arXiv preprint arXiv:2506.07339*, 2025.

Brohan, A., Brown, N., Carbalaj, J., Chebotar, Y., Dabis, J., Finn, C., Gopalakrishnan, K., Hausman, K., Herzog, A., Hsu, J., et al. Rt-1: Robotics transformer for real-world control at scale. *arXiv preprint arXiv:2212.06817*, 2022.

Chen, L., Zhao, H., Liu, T., Bai, S., Lin, J., Zhou, C., and Chang, B. An image is worth 1/2 tokens after layer 2: Plug-and-play inference acceleration for large vision-language models. In *European Conference on Computer Vision*, pp. 19–35. Springer, 2024.

Chen, Y. and Li, X. Rlrc: Reinforcement learning-based recovery for compressed vision-language-action models. *arXiv preprint arXiv:2506.17639*, 2025.

Dao, T., Fu, D., Ermon, S., Rudra, A., and Ré, C. Flashattention: Fast and memory-efficient exact attention with io-awareness. *Advances in neural information processing systems*, 35:16344–16359, 2022.

Intelligence, P., Black, K., Brown, N., Darpinian, J., Dhaballa, K., Driess, D., Esmail, A., Equi, M., Finn, C., Fusai, N., et al.  $\pi 0.5$ : a vision-language-action model with open-world generalization, 2025. URL <https://arxiv.org/abs/2504.16054>, 1(2):3.

Jabbar, J., Kim, D.-K., Smith, M., Patrikar, J., Ghosal, R., Wang, Y., Agha, A., Reddi, V. J., and Omidshafiei, S. Don't run with scissors: Pruning breaks vla models but they can be recovered. *arXiv preprint arXiv:2510.08464*, 2025.

Jin, T., Carbin, M., Roy, D., Frankle, J., and Dziugaite, G. K. Pruning's effect on generalization through the lens of training and regularization. *Advances in Neural Information Processing Systems*, 35:37947–37961, 2022.

Kim, M. J., Pertsch, K., Karamcheti, S., Xiao, T., Balakrishna, A., Nair, S., Rafailov, R., Foster, E., Lam, G., Sanketi, P., et al. Openvla: An open-source vision-language-action model. *arXiv preprint arXiv:2406.09246*, 2024.

Kim, M. J., Finn, C., and Liang, P. Fine-tuning vision-language-action models: Optimizing speed and success. *arXiv preprint arXiv:2502.19645*, 2025.

Le, Q., Diao, E., Wang, Z., Wang, X., Ding, J., Yang, L., and Anwar, A. Probe pruning: Accelerating llms through dynamic pruning via model-probing. *arXiv preprint arXiv:2502.15618*, 2025.

Li, Q., Liang, Y., Wang, Z., Luo, L., Chen, X., Liao, M., Wei, F., Deng, Y., Xu, S., Zhang, Y., et al. Cogact: A foundational vision-language-action model for synergizing cognition and action in robotic manipulation. *arXiv preprint arXiv:2411.19650*, 2024a.

Li, X., Hsu, K., Gu, J., Pertsch, K., Mees, O., Walke, H. R., Fu, C., Lunawat, I., Sieh, I., Kirmani, S., et al. Evaluating real-world robot manipulation policies in simulation. *arXiv preprint arXiv:2405.05941*, 2024b.

Liu, B., Zhu, Y., Gao, C., Feng, Y., Liu, Q., Zhu, Y., and Stone, P. Libero: Benchmarking knowledge transfer for lifelong robot learning. *Advances in Neural Information Processing Systems*, 36:44776–44791, 2023a.

Liu, Z., Wang, J., Dao, T., Zhou, T., Yuan, B., Song, Z., Shrivastava, A., Zhang, C., Tian, Y., Re, C., et al. Deja vu: Contextual sparsity for efficient llms at inference time. In *International Conference on Machine Learning*, pp. 22137–22176. PMLR, 2023b.

Liu, Z., Chen, Y., Cai, H., Lin, T., Yang, S., Liu, Z., and Zhao, B. Vla-pruner: Temporal-aware dual-level visual token pruning for efficient vision-language-action inference. *arXiv preprint arXiv:2511.16449*, 2025.

Ma, Y., Zhou, Y., Yang, Y., Wang, T., and Fan, H. Running vlas at real-time speed. *arXiv preprint arXiv:2510.26742*, 2025.

Shinde, G., Ravi, A., Dey, E., Sakib, S., Rampure, M., and Roy, N. A survey on efficient vision-language models. *Wiley Interdisciplinary Reviews: Data Mining and Knowledge Discovery*, 15(3):e70036, 2025.

Sun, M., Liu, Z., Bair, A., and Kolter, J. Z. A simple and effective pruning approach for large language models. *arXiv preprint arXiv:2306.11695*, 2023.

Wang, H., Xu, J., Pan, J., Zhou, Y., and Dai, G. Specprune-vla: Accelerating vision-language-action models via action-aware self-speculative pruning. *arXiv preprint arXiv:2509.05614*, 2025.

Wen, J., Zhu, Y., Li, J., Zhu, M., Tang, Z., Wu, K., Xu, Z., Liu, N., Cheng, R., Shen, C., et al. Tinyvla: Towards fast, data-efficient vision-language-action models for robotic manipulation. *IEEE Robotics and Automation Letters*, 2025.

Xu, S., Wang, Y., Xia, C., Zhu, D., Huang, T., and Xu, C. Vla-cache: Towards efficient vision-language-action model via adaptive token caching in robotic manipulation. *arXiv preprint arXiv:2502.02175*, 2025.

Yang, Y., Wang, Y., Wen, Z., Zhongwei, L., Zou, C., Zhang, Z., Wen, C., and Zhang, L. Efficientvla: Training-free acceleration and compression for vision-language-action models. *arXiv preprint arXiv:2506.10100*, 2025.

Yue, Y., Wang, Y., Kang, B., Han, Y., Wang, S., Song, S., Feng, J., and Huang, G. Deer-vla: Dynamic inference of multimodal large language models for efficient robot execution. *Advances in Neural Information Processing Systems*, 37:56619–56643, 2024.

Zhang, R., Dong, M., Zhang, Y., Heng, L., Chi, X., Dai, G., Du, L., Du, Y., and Zhang, S. Mole-vla: Dynamic layer-skipping vision language action model via mixture-of-layers for efficient robot manipulation. *arXiv preprint arXiv:2503.20384*, 2025.

## A. Experimental Settings

### A.1. VLA Model Details

**OpenVLA-OFT.** Derived from the OpenVLA architecture, OpenVLA-OFT incorporates an Optimized Fine-Tuning strategy that simultaneously enhances manipulation precision and computational efficiency. By adopting a continuous action space optimized via  $L1$  regression alongside parallel decoding and action chunking mechanisms, it achieves superior throughput and success rates on the LIBERO benchmark. A key characteristic of this variant is the deployment of bidirectional attention during inference.

$\pi_{0.5}$ .  $\pi_{0.5}$  is a generalist Vision-Language-Action (VLA) model designed to achieve broad open-world generalization in mobile manipulation by leveraging a heterogeneous co-training recipe. Building upon the  $\pi_0$  architecture and the PaliGemma VLM backbone,  $\pi_{0.5}$  integrates diverse data sources—including cross-embodiment robot data, multimodal web data, and high-level semantic predictions—to bridge the generalization gap. The model employs a hierarchical inference mechanism where it first predicts a high-level semantic subtask (e.g., "pick up the pillow") based on the visual observation and global instruction, which then conditions a specialized "action expert" to generate continuous low-level control actions via flow matching. This capability is developed through a two-stage training process that transitions from scalable discrete token pre-training to precise continuous flow-matching post-training, enabling the execution of complex, long-horizon tasks in environments completely unseen during training.

**CogACT.** This architecture synthesizes perception and reasoning by employing DINOv2 and SigLIP for visual encoding alongside a Llama2-7B language backbone. To bridge the gap between high-level cognition and low-level action, CogACT utilizes a specialized Diffusion Transformer (DiT). By conditioning this diffusion-based action module on the features extracted by the VLM, the model effectively addresses the challenges of generating precise, continuous, and temporally correlated robotic trajectories.

### A.2. Acceleration Method Details

**FastV.** FastV addresses inference latency in Large Vision-Language Models (LVLMs) by mitigating visual token redundancy. The method is grounded in the observation that deep layers often exhibit an attention sink phenomenon, where visual tokens consume substantial computational resources despite receiving minimal attention weights. To counter this, FastV introduces a plug-and-play mechanism that monitors attention scores to dynamically discard low-utility visual tokens after a certain depth, thereby reducing FLOPs while preserving model accuracy.

**VLA-Cache.** VLA-Cache is a training-free inference accelerator tailored for robotic VLA models. It exploits the observation that visual scenes in robotic tasks remain largely stable between consecutive frames, particularly in background areas. By distinguishing between static and dynamic elements, the method recycles KV-cache states for unchanged tokens while enforcing full computation for critical, task-relevant features to ensure precision. Furthermore, it incorporates an adaptive strategy that modulates the caching ratio according to layer-specific attention patterns.

### A.3. Implementation Details

For OpenVLA-OFT, we set the sensitivity parameter  $p = 5$ . Regarding temporal inertia parameter, we set  $\alpha = 0.7$  for LIBERO-Spatial and LIBERO-Long to reduce historical reliance in dynamic spatial layouts. Conversely, for LIBERO-Object and LIBERO-Goal, we use a higher  $\alpha = 0.9$  as these manipulation tasks feature relatively stable environments. For  $\pi_{0.5}$ , given its enhanced execution stability, we set the sensitivity parameter to 80 to mitigate environmental noise. The temporal inertia parameter is kept fixed at 0.7. For CogACT, we set the sensitivity parameter  $p = 5$ ,  $\alpha = 0.7$ .

### A.4. Benchmarks Details

**Real-Robot Setup.** We conducted experiments on a 7-DoF Kinova Gen3 robotic arm, with the hardware setup shown in Fig.7. Our system uses two Intel RealSense D435i cameras: one providing a third-person view and the other mounted on the wrist.

**Training Details.** For each task, we collected 50 demonstrations. When fine-tuning the  $\pi_{0.5}$  model, we froze the VLM backbone and performed LoRA-based adaptation only, while fully fine-tuning the action expert. We used a global batch size of 32 and trained for 10k steps on a single GPU.

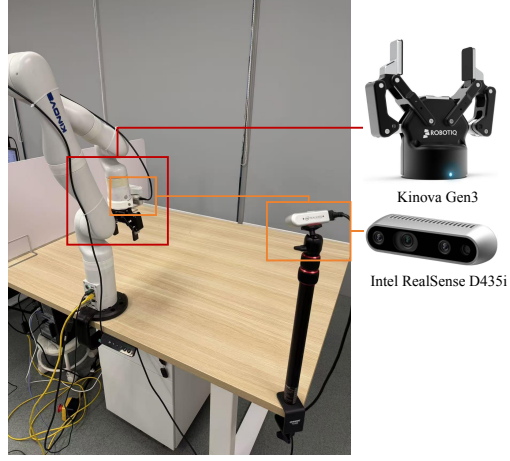


Figure 7. Kinova Gen3 Robot Setup.

## B. Real-robot Analysis

We conduct experiments on a real-robot platform. Specifically, we fine-tune  $\pi_{0.5}$  on our collected dataset, training each task for 10,000 steps with a batch size of 32. During evaluation, to more thoroughly assess the model’s capability, we test on 20 randomly sampled object placements within the training range, re-randomizing the object position in every trial to probe the model’s spatial reasoning and generalization across object locations. On real-robot tasks, while achieving a  $1.26\times$  speedup, EcoVLA exhibits a minor performance drop compared to  $\pi_{0.5}$ . We further observe that most failures occur when the object is placed near the boundary of the workspace. We conjecture that such edge-case placements require finer-grained spatial cues and stricter geometric constraints, making the pruned model more susceptible to representation loss and thus less robust in spatial generalization.

## C. Hyperparameter Analysis

We evaluate the influence of sensitivity parameter  $p$  and temporal inertia parameter,  $\alpha$  on success rates using  $\pi_{0.5}$ .

**Impact of Sensitivity Parameter.** As shown in Fig.6 (b), we evaluate the impact of the sensitivity parameter  $p$ , as it directly dictates EcoVLA’s responsiveness to environmental dynamics. At low  $p$  values, EcoVLA adopts a conservative strategy, updating sparsity patterns only during drastic environmental changes, thereby overlooking subtle cues. Conversely, an excessively high  $p$  induces hypersensitivity, where sensor noise or lighting fluctuations are misidentified as dynamics. This triggers redundant updates that disrupt temporal continuity. Performance peaks at  $p = 80\%$ , a setting that effectively filters noise while retaining sufficient sensitivity to capture physical transitions, ensuring robust operation in complex environments.

**Impact of Temporal Inertia Parameter.** We investigate the properties of  $\alpha$  on LIBERO-Long (Fig.6 (a)), as this parameter is critical for long-horizon tasks with varying spatial layouts. High  $\alpha$  excessively weights history, causing the model to miss new critical features, whereas extremely low  $\alpha$  relies on single-frame inputs, disrupting inference stability. Performance peaks at 87.0% with an intermediate  $\alpha$ , validating our Temporal Consistency Pruning strategy. This confirms that EcoVLA effectively filters high-frequency noise while maintaining sensitivity to environmental dynamics.